Symmetry energy from two-nucleon separation energies of Pb and Ca isotopes

Myeong-Hwan Mun ◉ and Myung-Ki Cheoun ◉*

Department of Physics and Origin of Matter and Evolution of Galaxies (OMEG) Institute, Soongsil University, Seoul 06978, Korea

Eunja Ha

Department of Physics and Research Institute for Natural Science, Hanyang University, Seoul 04763, Korea

H. Sagawa

*RIKEN, Nishina Center for Accelerator-Based Science, Wako 351-0198, Japan
and Center for Mathematics and Physics, University of Aizu, Aizu-Wakamatsu, Fukushima 965-8560, Japan*

Gianluca Colò

Dipartimento di Fisica, Università degli Studi, and INFN sezione di Milano, via Celoria 16, 20133 Milano, Italy

We investigate the symmetry energy in relation with the two-proton and two-neutron separation energies using different nuclear mass data. For this aim, we exploit the deformed relativistic Hartree-Bogoliubov theory in the continuum (DRHBc), FRDM2012, and AME2020 data. First, we study the two-proton and two-neutron separation energies in Pb and Ca isotopes by subtracting the contribution of Coulomb energy. They show a strong correlation with neutron number as well as with the neutron skin thickness. By taking the relative difference of both separation energies, we derive the symmetry energy from Ca and Pb isotopes. Since the nuclear surface contributes to the symmetry energy, we deduce the volume symmetry energy by subtracting the surface contribution using several mass models. The obtained symmetry energy coefficient, a_{sym}, is 20.0–22.7 MeV for Pb isotopes and 18.7–19.3 MeV for Ca isotopes from the DRHBc mass table data, while the results from other mass tables are 19.6–22.1 (20.7–22.3) MeV for Pb isotopes and 18.9–19.0 (19.6–19.7) MeV for Ca isotopes from AME2020 (FRDM2012) data. The volume contribution to the asymmetry coefficient, a_{sym}^{v}, which depends on the ratio of the surface to the volume energy coefficients, a_s/a_v, is also provided for each mass model. Since the ratio a_s/a_v is determined neither by nuclear theory nor by experimental data, we have investigated a_{sym}^{v} by using the ratio a_s/a_v as a free parameter, and have obtained $a_{\mathrm{sym}}^{v} = 27.0$ MeV, almost irrespective of nuclear model and isotopic chain, with the ratio a_s/a_v constrained as $a_s/a_v = 1.10$–1.13.

I. INTRODUCTION

The neutron skin thickness (NST) of neutron-rich nuclei has been one of the most important topics in nuclear physics because it can provide critical information on the symmetry energy in finite nuclei, as well as on the structure of neutron stars. There are several experimental datasets available for the NST, including parity-violating electron scattering, i.e. the results from PREX I, PREX II, and CREX experiments, as well as data on the dipole polarizability obtained by proton elastic scattering and antiproton scattering [1–5]. From the viewpoint of the symmetry energy, the NST is a significant observable because it is proportional to the slope parameter of the equation of state (EoS) of nuclear matter [6].

In this work, we focus on the proton and neutron separation energy because the proton separation energy implies the propagation of protons in the NST region, and consequently it is affected by the NST, while the neutron separation energy becomes smaller with the increase of the neutron number due to the more dilute neutron density in the NST. Specifically, we utilize two-neutron and two-proton separation energies in even-even Pb and Ca isotopes because one-proton and one-neutron separation energies require one to consider the additional pairing energy of even-odd nuclei and the Pauli blocking. In addition, since the Coulomb energy is crucial to determine the proton separation energy, we need to subtract the contribution from those separation energies to discuss the symmetry energy of finite nuclei. Furthermore, for the symmetry energy in nuclear matter, we derive the volume symmetry energy coefficient subtracted by the surface contribution.

By using the mass table of the deformed relativistic Hartree-Bogoliubov in continuum (DRHBc) model, which attained more neutron-rich and proton-rich nuclei than other nuclear mass models, we deduce the two-nucleon separation energies in a wide mass region, including nuclei near the drip lines, and extend this process to other mass model

TABLE I. Comparison of the NST to the experimental data in the unit of fm. The value of E_p for Ca is 295 MeV, and there are different values, namely 295, 650, and 800 MeV, for ^{208}Pb [2–4]. The antiproton scattering data are from Ref. [45].

	DRHBc	p-elastic scatt. data (E_p) (MeV)	PREX II and CREX	$\bar{p}$ data
^{40}Ca	−0.043	$-0.010^{+0.022}_{-0.024}$ (295)		
^{48}Ca	0.223	$0.168^{+0.025}_{-0.028}$ (295)	$0.121 \pm 0.026(\text{exp}) \pm 0.024(\text{model})$	0.090 ± 0.050
		$0.211^{+0.054}_{-0.063}$ (295)		
^{208}Pb	0.257	0.20 ± 0.04 (650)	0.283 ± 0.071	
		0.14 ± 0.04 (800)		

data to come out with a realistic estimate of the systematic uncertainties in our extraction. Then, the difference has an explicit relation with the asymmetry energy coefficient, a_{sym}, in the semiempirical Bethe-Weizsäcker liquid drop mass model. Based on the Bethe-Weizsäcker mass formula [7], the total binding energy of a nucleus is written as

$$E_B(A, Z) = a_v A - a_s A^{2/3} - a_c \frac{Z^2}{A^{1/3}} - a_{\text{sym}} I^2 A, \quad (1)$$

for a nucleus with mass number A and proton number Z. In Eq. (1), a_v, a_s, a_c, and a_{sym} are the volume, surface, Coulomb, and symmetry energy terms, respectively. $I = (N - Z)/A$ represents the isospin asymmetry and the pairing energy term is discarded since it does not play any role in our further considerations. Here, we use minus signs except for the volume term, by which the binding energy and all coefficients are positive, because the surface, Coulomb, and symmetry energies tend to unbind the nucleus. By subtracting the Coulomb energy, we define a modified binding energy formula without the Coulomb contribution as

$$E_B^*(A, Z) = E_B(A, Z) + a_c \frac{Z^2}{A^{1/3}} = a_v A - a_s A^{2/3} - a_{\text{sym}} I^2 A. \quad (2)$$

Then, the separation energies without the Coulomb energy term are given by

$$\begin{aligned} S_{2n}^* &= [E_B^*(A, Z) - E_B^*(A - 2, Z)], \\ S_{2p}^* &= [E_B^*(A, Z) - E_B^*(A - 2, Z - 2)]. \end{aligned} \quad (3)$$

The difference between the corrected $2p$ and $2n$ separation energies can be expressed in term of the isospin asymmetry coefficient as

$$S_{2p}^* - S_{2n}^* = a_{\text{sym}} \frac{8(N - Z)}{(A - 2)} = 8 a_{\text{sym}} I^*, \quad \text{with } I^* = \frac{N - Z}{A - 2}. \quad (4)$$

For the application to nuclear matter, we divide the symmetry energy into the volume and surface part (a_{sym}^s, a_{sym}^v), using the following relation [8]: $a_{\text{sym}} I^2 A = (a_{\text{sym}}^v A + a_{\text{sym}}^s A^{2/3}) I^2$. Then Eq. (4) is reexpressed as

$$\begin{aligned} S_{2p}^* - S_{2n}^* &= 8 I^* \left(a_{\text{sym}}^v + a_{\text{sym}}^s (A - 2)^{-1/3} \right) \\ &= 8 I^* a_{\text{sym}}^v \left(1 - \frac{a_s}{a_v} (A - 2)^{-1/3} \right), \end{aligned} \quad (5)$$

where we define the ratio of the surface to the volume term as $a_{\text{sym}}^s / a_{\text{sym}}^v = -a_s/a_v$ [8].

We take a_v and a_s, whose values depend on the nuclear model, as summarized at Table II in Appendix D of Ref. [8]. We have performed calculations for Pb and Ca isotopes using the DRHBc model [9], the finite-range droplet model (FRDM2012) model [10], and the Atomic Mass Evaluation (AME2020) data [11]. The results show an interesting consequence for the symmetry energy in finite nuclei.

Before the discussion on the symmetry energy, we add a few comments on the mass models exploited in this work. The AME2020 data [12] is the result, as the name hints, of the evaluation of experimentally measured masses. FRDM is a global nuclear mass model, combining a liquid-drop mass model for the macroscopic energy with microscopic shell corrections based on the Strutinsky procedure. In particular, FRDM2012 data [13] predicts the masses of more than 2000 nuclei with a high accuracy: the root-mean-square (rms) deviation with respect to the experiment is $\sigma_{\text{rms}} = 0.560$ MeV. The price to pay for this high accuracy is a large number of parameters which are optimized to reproduce accurately the experimental binding energies.

DRHBc is a covariant version of nuclear density functional theory (DFT). It is based on a microscopic, point-coupling realization of an energy density functional and it has been improved and tuned to include superfluidity. Its practical implementation includes deformation, and coupling to the continuum which is relevant to describe properly nuclei close

TABLE II. Formulas for the Coulomb energy corrections to Eq. (1) in Ref. [47], where the differences of experimental binding energies between 88 pairs of mirror nuclei (with the same mass number A, but with neutrons and protons interchanged) are adopted to fix the parameters a_c and b in the mass region $11 \leqslant A \leqslant 75$, based on the AME2012 data [48]. Sets I (III) and II (IV) are obtained by fitting the data, respectively, without and with the Coulomb exchange term [including the proton self-interaction correction $Z(Z - 1)$]. The last column σ provides the rms deviations from the fitting procedure.

	Coulomb energy E_c	a_c (MeV)	b	σ (keV)
Set I	$a_c \frac{Z^2}{A^{1/3}}$	0.625		336
Set II	$a_c \frac{Z^2}{A^{1/3}}(1 - bZ^{-2/3})$	0.715	1.374	121
Set III	$a_c \frac{Z(Z-1)}{A^{1/3}}$	0.642		249
Set IV	$a_c \frac{Z(Z-1)}{A^{1/3}}(1 - bZ^{-2/3})$	0.704	0.985	118

to the drip lines. Although the model has parameters extracted from a fit, these are associated with microscopic coupling constants and there is no *ad hoc* parameter that betrays the basic DFT philosophy: in this respect, it is a microscopic model and not a mass model. While it is fair to discuss these models in an objective way, and let the reader have an opinion about their pros and cons, we note that it is not guaranteed that a model having more parameters and smaller errors when compared to experimental masses necessarily allows a more accurate extraction of the symmetry energy from the data.

This paper is organized as follows. A brief description of the DRHBc theory used in the present calculation is presented in Sec. II. Detailed results of Pb and Ca isotopes including the NST and the nucleon separation energies are provided in Sec. III. Finally, the summary and conclusion are given in Sec. IV.

II. FORMALISM

In order to see the consequences of the above discussion, we need a well-refined nuclear model which has to incorporate the deformation, the pairing correlations and the continuum, through a microscopic approach, so that it can account well for properties of the nuclear masses as a whole, by covering nuclei near the drip lines. Another important ingredient is the relativistic description which has been initiated by the authors in Refs. [14,15] with various meson-exchange models inside nuclei, and has enabled us to incorporate consistently the nucleonic spin degree of freedom.

Along this line, the DRHBc theory was developed for deformed halo nuclei in Refs. [16,17], and recently extended [18] with point-coupling density functionals. This theory is proved to be capable of providing a good description of the nuclear masses with high predictive power [9,19,20], and it has successfully been applied to some particular nuclei [21–28]. It follows the previous relativistic continuum Hartree-Bogoliubov (RCHB) approach, calculated in coordinate space [29,30] by explicitly including the deformation in a Dirac Woods-Saxon basis [31]. Here we note that the deformed cylindrical basis preserving axial symmetry could be an alternative to effectively treat the convergence of the total energy as argued in Ref. [32], where the Gogny-type pairing force was exploited for neutron rich nuclei near drip lines and odd nuclei.

In this work, we focus on the two-nucleon separation energies and NST of the Pb and Ca isotopes within the DRHBc theory, which was succinctly summarized in Refs. [17,18], as well as the nuclear mass data of AME2020 and FRDM. The present calculations are carried out in the relativistic Hartree-Bogoliubov theory with the density functional PC-PK1 [33],

$$\begin{pmatrix} h_D - \lambda & \Delta \\ -\Delta^* & -h_D^* + \lambda \end{pmatrix} \begin{pmatrix} U_k \\ V_k \end{pmatrix} = E_k \begin{pmatrix} U_k \\ V_k \end{pmatrix}, \quad (6)$$

where h_D, λ, E_k, (U_k, V_k) are the Dirac Hamiltonian, the Fermi energy and the quasiparticle energy and wave function, respectively. The pairing potential Δ is given as a function of

the pairing tensor $\kappa(\mathbf{r}, \mathbf{r}')$ as follows:

$$\Delta(\mathbf{r}, \mathbf{r}') = V(\mathbf{r}, \mathbf{r}')\kappa(\mathbf{r}, \mathbf{r}'), \quad (7)$$

with a density-dependent zero range force

$$V(\mathbf{r}, \mathbf{r}') = \frac{V_0}{2}(1 - P_\sigma)\delta(\mathbf{r} - \mathbf{r}')\left(1 - \frac{\rho(\mathbf{r})}{\rho_{\mathbf{sat}}}\right). \quad (8)$$

For the pairing strength, we use $V_0 = -325.0$ MeV fm^3. The saturation density is adopted as $\rho_{\text{sat}} = 0.152$ fm^{-3}, together with a pairing window $E_{\text{cut}}^{q,p} = 100$ MeV. The energy cutoff $E_{\text{cut}}^+ = 300$ MeV and the angular momentum cutoff $J_{\text{max}} = (23/2)\hbar$ are taken for the Dirac Woods-Saxon basis. The above numerical details are the same as those suggested in Refs. [18,20] for the DRHBc mass table calculation. For the present calculation of the Pb (Ca) isotopes, the Legendre expansion truncation is chosen as $\lambda_{\text{max}} = 8$ (6) [18,20].

Empirical pairing gaps of Pb isotopes were shown to be properly reproduced with the energy cutoff, the maximum angular momentum, and the Legendre expansion truncation obtained from the convergence check of total energies, as shown in Fig. 5(b) in Ref. [18].

The present zero-range scheme for the pairing force is better than the simple constant gap approximation, but it has still the pairing window problem in the pairing tensor, as discussed in Refs. [34,35], because it needs an arbitrary energy cut-off parameter for neutron-rich nuclei. In spherical nuclei, the neutron pairing gaps are well reproduced by the pairing window defined by $E_{\text{cut}}^{q,p} = 100$ MeV. But for deformed nuclei $A = 186$–198 (see Fig. 2 in Ref. [36]) the results of $E_{\text{cut}}^{q,p} = 200$ MeV are better than those by using other windows. This implies that the convergence of total energies with the pairing windows has to be more carefully assessed in the case of deformed nuclei. We leave it as a future work. A more elaborate approach for the pairing interaction, beyond the zero-range scheme, is that based on the Gogny-type finite-range pairing force [37], using a separable approximation [38,39]. This kind of treatment of pairing interaction is also applied to the covariant density functional theory adopted for studying neutron-rich nuclei in Refs. [40–43].

III. RESULTS AND DISCUSSION

A. Two-neutron and two-proton separation energies

Both the DRHBc and RCHB results show a clear correlation between the NST and the neutron number, as shown in Fig. 1. The small deviation of the RCHB results [44] in Pb isotopes, with respect to the DRHBc results, can be attributed to the fact that the RCHB model does not consider explicitly the deformation [9].

We obtain the NST values of ^{40,48}Ca equal to -0.043 and 0.223 fm, respectively, in the DRHBc model. For ^{208}Pb, the DRHBc value is 0.257 fm. We compare these results with various experimental findings both in Fig. 1 and in Table I. An interesting point is that ^{208}Pb data from proton elastic scattering experiments show systematically smaller NST than the data from PREX II and than the results of the present calculations. On the other hand, such data are consistent with the dipole polarization experiments and also with
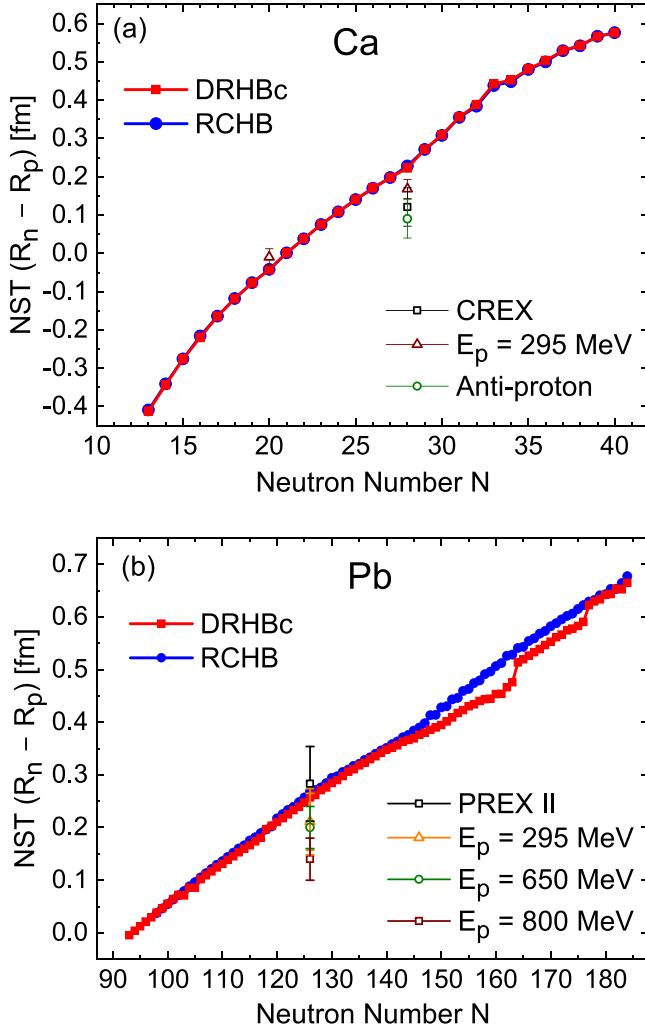
FIG. 1. Evolution of NST for Ca (a) and Pb (b) isotopes. We obtain the NST for ^{208}Pb as $R_n - R_p = 0.257$ fm and the NST for ^{40}Ca as $R_n - R_p = -0.043$ fm in the DRHBc results. Data from different experiments (CREX and PREX II, antiproton scattering, and proton elastic scattering at different incident proton energies E_p) are also displayed, and detailed in Table I. In theoretical studies, DRHBc takes into account both the continuum and the deformation, while RCHB includes only the continuum effect.

FIG. 2. (a) Evolution of the NST, S_{2p} and S_{2n} obtained by DRHBc [9] and RCHB [44] with the neutron number (denoted by squares, circles, and triangles, respectively) for Pb isotopes. S_{2p} and S_{2n} are compared to the AME2020 data (denoted as stars) [12]. (b) Evolution of S_{2n} and S_{2p} with the NST.

nonrelativistic Skyrme calculations. Curiously, the NST from proton scattering data of ^{48}Ca is larger than that of CREX data, but smaller than the DRHBc results. While there might be model dependence related to the optical model adopted in the analysis of the proton elastic scattering data, the difficulty of reconciling PREX and CREX data is still an interesting and open problem.

Figure 2(a) demonstrates the evolution of the NST, the two-neutron separation energy (S_{2n}), and two-proton separation energy (S_{2p}) with the neutron number for Pb isotopes with the available separation energy data. Figure 2(b) shows the separation energy evolution with the NST. All observables show clear correlations with the neutron number as well as the NST. S_{2n} decreases with the neutron number and shows an
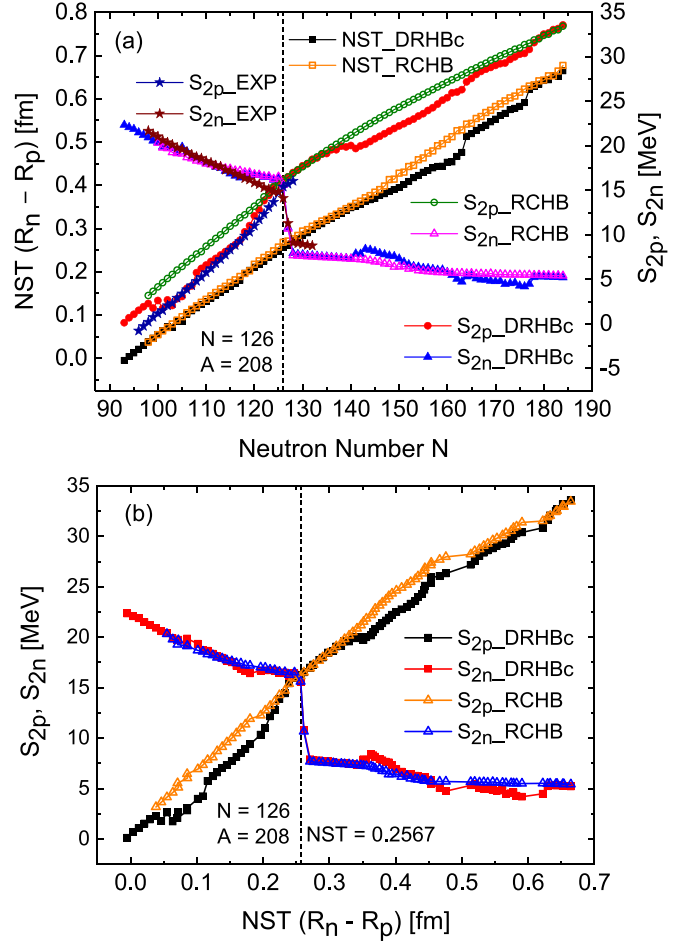
abrupt decrease at the neutron magic number $N = 126$. This is an indication of the magic shell structure.

We also note an almost monotonic increase of S_{2p} with the neutron number. With the increase of the NST by the increase of neutron number, because of the strong proton-neutron interaction, the proton potential is more deepened, and consequently S_{2p} increases. This can also be explained by the increase of Fermi energy difference between proton and neutron, $\epsilon_p - \epsilon_n$, as discussed in Ref. [46]. Furthermore, the monotonic increase of S_{2p} with the neutron number implies that the NST, as well as the slope parameter of the symmetry energy, are closely related to the behavior of S_{2p}, which will be discussed in detail later on.

Figure 2(a) also demonstrates the evolution of the NST with the neutron number. In particular, Fig. 2(a) shows different increase rates of the NST and S_{2p}. Further, since the neutron number and the NST also have a correlation, we show the evolution of the S_{2p} and S_{2n} with the NST in Fig. 2(b).

Other NST calculations by the RCHB model [29,30] show more straight correlations to the neutron number, and the separation energies also display a pattern similar to that of
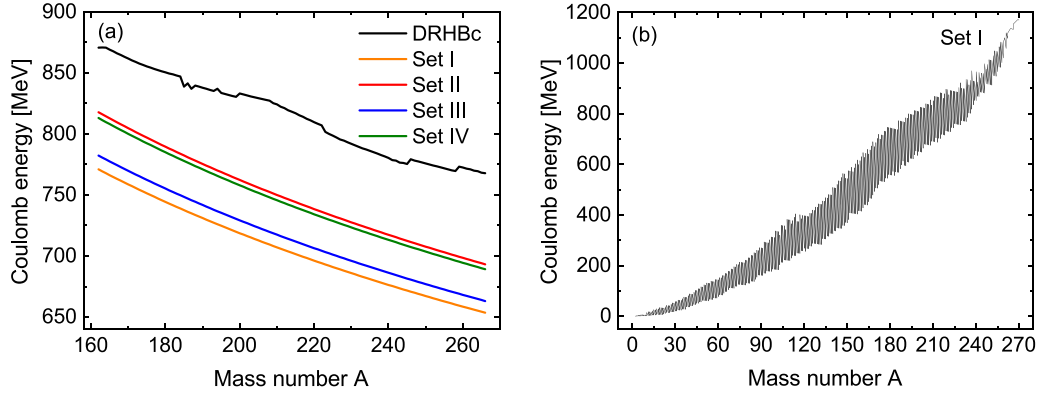
FIG. 3. Coulomb energies of Pb isotopes (a). Sets I–IV in Table II are taken from Ref. [47] and the DRHBc Coulomb energies are taken from Ref. [9]. The Coulomb energy data in the panel (b) are calculated for all isotopes, for a given mass number A, using Set I. The Coulomb energies of all isobars for a given mass number A are indicated explicitly.

the NST. The smooth correlations displayed by the RCHB results stem from the lack of deformation in these calculations. Hereafter, we focus on the evolution of S_{2n} and S_{2p} with the neutron number. A detailed discussion of the relation to the NST will be presented in a forthcoming paper, with the additional analysis of the symmetry energy in nuclear matter.

B. Coulomb energy correction

Since the Coulomb energy affects the proton separation energy, we subtract the Coulomb energy. Following the prescriptions used in Ref. [47], which are summarized in Table II, we show the evolution of the Coulomb energy of Pb isotopes as well as that of the DRHBc calculation in Fig. 3. The Coulomb energy decreases with the mass number, as expected. We also note that Sets I and III are characterized by a Coulomb energy which is about 40–50 MeV smaller than for Sets II and IV. This comes from the fact that the exchange Coulomb energy cancels with the direct Coulomb energy, but the a_c values themselves in Sets II and IV are larger than those in Sets I and III. Here we note that the isospin symmetry breaking interactions are not included in the results of Fig. 3.

The Coulomb energy by using the DRHBc is presented with the black curve, and the values are much larger than all those obtained with Sets I–IV in Table II. In fact, these include the Coulomb exchange energy, either explicitly (Sets II and IV) or implicitly (Sets I and III). Therefore, more refined calculations of the Coulomb exchange term might be desirable for more exact access of the Coulomb energy, because the Coulomb exchange interaction is not included in the DRHBc model. The small discontinuous Coulomb energy by the DRHBc comes from the deformation of Pb isotopes. The Coulomb energy per proton in Pb isotopes, from the DRHBc model, decreases from about 11 to 8 MeV along the $^{162-266}$Pb isotopes. Figure 3(b) shows an example of the Coulomb energy from the Set I in the whole mass table: it increases with the mass number as expected. The spread in each isobaric chain amounts to a few tens of MeV. It means that the Coulomb energy correction is important in the present calculation.

Figure 4(a) shows the two-nucleon separation energy (S_{2p} and S_{2n}) and the Coulomb-corrected one (S_{2p}^* and S_{2n}^*). S_{2p}^* is larger, by about 36 MeV on average, than S_{2p}. We can find a clear correlation of S_{2p} and S_{2p}^* with the neutron number, that is, even when the Coulomb energy is subtracted. The uncertainty from the Coulomb energy estimated from the difference between Sets I and II in Table II turns out to be about 5 MeV. Here we do not take into account the irregular pattern due to the deformation in the upper curves in Fig. 4(a). We also present the experimental separation energy from AME2020 data [11] and their Coulomb-corrected values.

S_{2p} and S_{2n} show an X-type crossing behavior at the point near the magic shell $N = 126$, while S_{2p}^* and S_{2n}^* cross at the magic number $N = 82$ in panel (a). We note that S_{2n}^* is also affected by about 2–3 MeV by the Coulomb energy subtraction, because of the change of the total binding energies. Figure 4(b) show the evolution of the difference of S_{2p}^* and S_{2n}^* for Pb isotopes, as a function of the neutron number N.

The differences between S_{2p}^* and S_{2n}^* in Figs. 4(b) and 4(c) are found to be linearly proportional to the neutron number N, and also to $I^* = (N - Z)/(A - 2)$, except at the shell closure and in the deformed region. This difference should be constant with respect to $8I^*$ according to the formula in Eq. (4), and the constant is directly related to the asymmetry coefficient a_{sym} in the mass formula. Although we can see large fluctuations, we extracted the value a_{sym} from Fig. 4(d) by taking a fit to the data. In the fitting process, we discarded the region $I^* < 0.100$, because it is the proton-rich region, and also the $0.217 < I^* < 0.271$ region, because it is the region near the magic number. In order to extract the symmetry energy coefficient, we have to subtract the shell corrections in the vicinity of magic shells, which usually has been done by the Strutinsky method [49]. Here we adopt a prescription simply to discard the results near magic shells, which is equivalent to a smooth continuation approach, i.e., subtracting the Fermi energy difference of nuclei before and after the shell closure. The values of a_{sym} from Pb isotopes are shown in Fig. 4(d): these span the interval between 20.0 and 22.7 MeV, depending on how the Coulomb correction is implemented. Detailed values are in Table III.
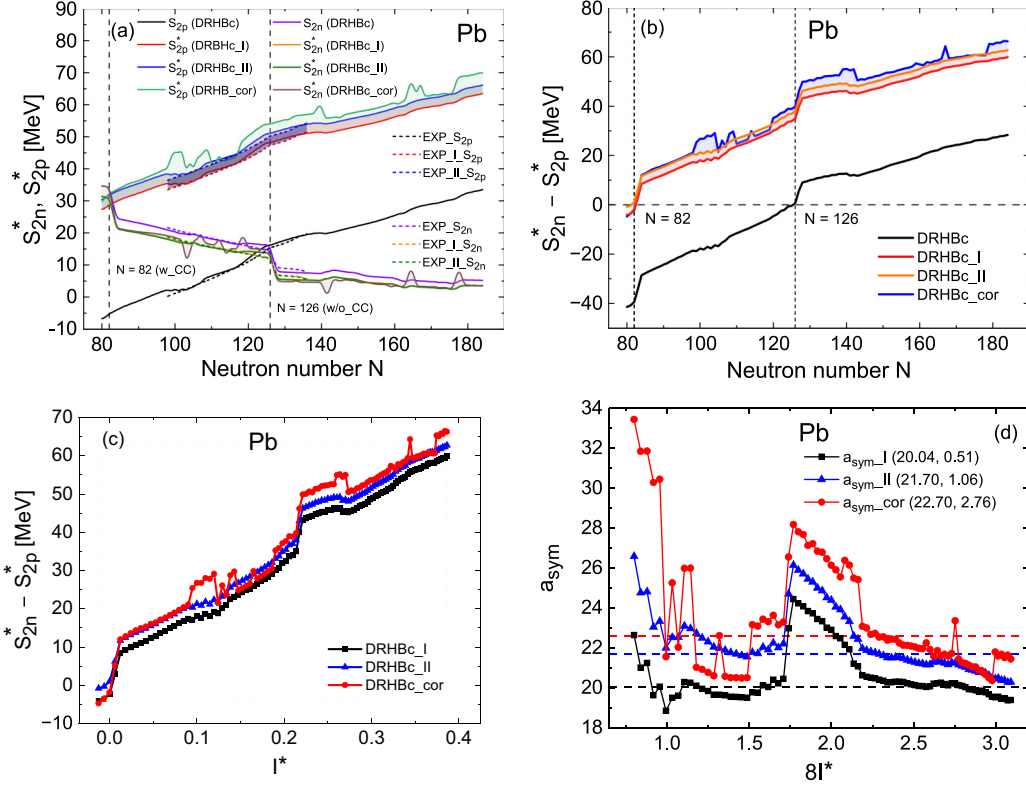
FIG. 4. (a) Evolutions of S_{2p}, S_{2p}^*, S_{2n}, and S_{2n}^* as a function of the neutron number N and (b) the difference $S_{2p}^* - S_{2n}^*$ for the Pb isotopes. The S_{2p}^* and S_{2n}^* are those including the Coulomb energy correction. The shaded regions indicate the uncertainty due to the difference between Sets I and II for the Coulomb correction. DRHBc_I and DRHBc_II label the results obtained by subtracting the Coulomb energy from Sets I and II. DRHBc_cor is the result obtained by subtracting the Coulomb energy calculated by the DRHBc model itself. EXP are the experimental data from AME2020. EXP_I and EXP_II are the data corrected by subtracting the Coulomb energy from Sets I and II. Panels (c) and (d) show the difference $S_{2p}^* - S_{2n}^*$ as a function of $I^* = (N - Z)/(A - 2)$, and a_{sym} with respect to $8I^*$, respectively. The numbers in the parentheses in panel (d) are the central values of a_{sym} and their rms deviations. Here we show only the results from Sets I and II for simplicity.

In the following, we present the S_{2p}^* and S_{2n}^* results for Ca isotopes in Fig. 5. The general behavior is very similar to that in Pb isotopes. We found also the X-type band of S_{2p} and S_{2n} as well as S_{2p}^* and S_{2n}^* in Fig. 5(a). An interesting point is the change of the crossing point without and with the Coulomb energy. With the Coulomb energy subtraction, the crossing point moves to the magic number $N = 20$ for S_{2p}^* from $N = 22$ for S_{2p}. This is very similar to the results for Pb isotopes in the vicinity of the magic number $N = 82$ and 126. This tendency implies that both separation energies, S_{2p}^*

TABLE III. Results of extracted a_{sym} for Ca and Pb with DRHBc, AME2020, and FRDM2012 data. The numbers in parentheses are the rms deviations.

	DRHBc	AME2020	FRDM2012
Ca_a_{sym}_I	18.70 (1.23)	18.96 (0.73)	19.66 (0.48)
Ca_a_{sym}_II	18.69 (1.22)	18.93 (0.72)	19.65 (0.47)
Ca_a_{sym}_cor	19.34 (1.31)		
Pb_a_{sym}_I	20.04 (0.51)	19.60 (0.41)	20.67 (0.76)
Pb_a_{sym}_II	21.70 (1.06)	22.15 (0.68)	22.33 (0.41)
Pb_a_{sym}_cor	22.70 (2.76)		

and S_{2n}^*, are the same for $N = Z$ nuclei, and that the present approach is very reasonable.

However, the crossing points of S_{2p} and S_{2n} (or S_{2n}^*) are at $N = 126$ and $N = 22$, respectively, for Pb and Ca isotopes. Other results from Sets III and IV show similar features. Even the results of AME and FRDM model do not provide different outcome. Since $N = 126$ for ^{208}Pb is the magic number, the value $N = 22$ is a bit difficult to understand.

The relative difference $S_{2p}^* - S_{2n}^*$ in Ca isotopes, in Figs. 5(b) and 5(c), shows also a clear correlation with the neutron number and I^*. The a_{sym} from Fig. 5(d) is estimated as about 18.7–19.7 MeV, and these values are a bit smaller than those from the Pb isotopes. In the fitting we also discarded the region around $I^* = 0$, corresponding to the $N = Z = 20$ case. The final a_{sym} values fitted from Figs. 4(d) and 5(d) are also tabulated in Table III with the results of other mass tables, AME2020 and FRDM2012. In particular, we note that the DRHBc_cor value is larger, by about 1 MeV, than those from the other Coulomb corrected results using Sets I and II.

C. Surface symmetry energy correction

Hereafter, we will disentangle the contribution of the surface symmetry energy to a_{sym} by comparing the two results
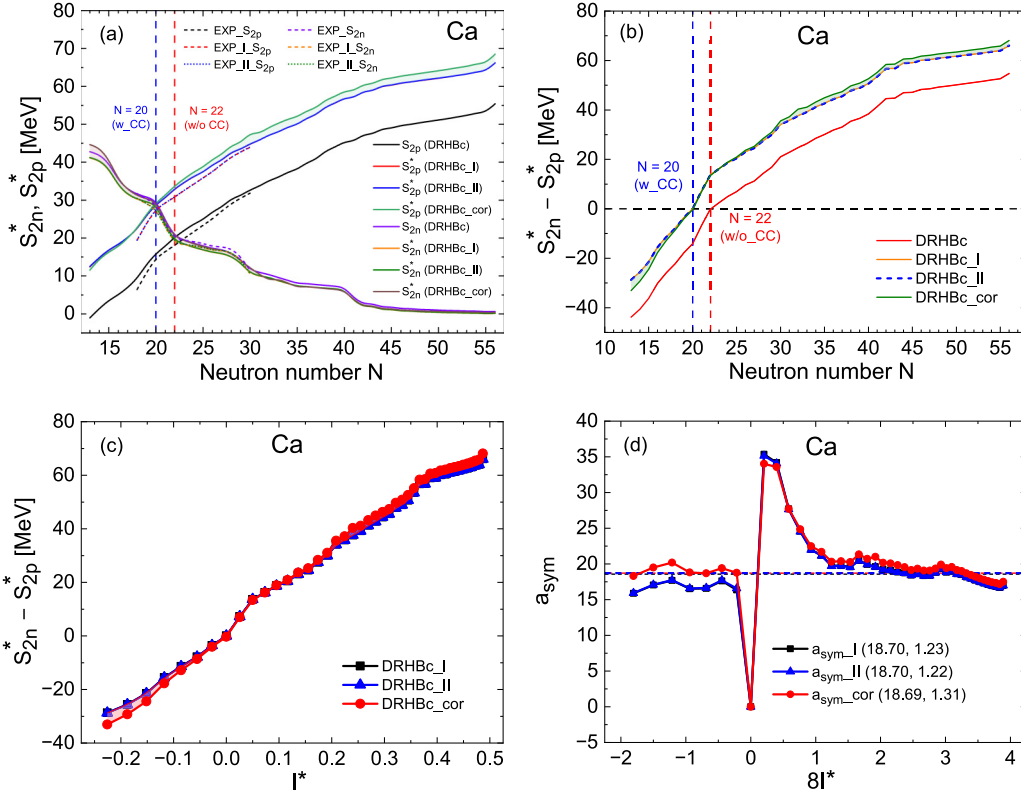
FIG. 5. Same as Fig. 4, but for Ca isotopes. The numbers in parentheses are the central values and the rms deviations.

of Pb and Ca isotopes. We will try to extract a model-independent a_{sym}^v value. We use the $S_{2p}^* - S_{2n}^*$ formula given by Eq. (5), which divides the symmetry energy into volume (a_{sym}^v) and surface (a_{sym}^s) parts. By using the ratio of a_s/a_v from nuclear models [8], we deduce the a_{sym}^v values and tabulate them in Table IV.

If we compare the results in Table III to those in IV (see the first six rows for the DRHBc case), the a_{sym}^v value is increased compared to the a_{sym} value by about 7.5 MeV for Ca and 4.5 MeV for Pb isotopes, due to the surface symmetry energy (a_{sym}^s) correction, in the DRHBc model case. If we use a bit larger value of a_s/a_v, from FRDM, the change amounts to a larger value, 10.86 and 6.62 MeV for Ca and Pb isotopes. It is interesting that the corrections for Ca isotopes are larger than those by Pb isotopes. It suggests that the surface contribution to the symmetry energy becomes larger in light nuclei rather than in heavy nuclei as expected from Eq. (5).

D. Results from other mass models

Here we perform the evaluation of $S_{2p}^* - S_{2n}^*$ and a_{sym} for Ca and Pb by using each of the nuclear mass models, AME2020 and FRDM2012. For example, Fig. 6 presents the results of $S_{2p}^* - S_{2n}^*$ and a_{sym} from other mass models. We note that the results by AME2020 and FRDM2012 are lower than those by DRHBc. The final results for a_{sym}^v, corrected by the surface contribution, are tabulated in Table IV for the nuclear mass models. The results for a_{sym}^v depend on

TABLE IV. Macroscopic parameters (a_s/a_v) deduced from different mass formulas [8], and the results of a_{sym}^v extracted after correcting a_{sym} by the surface contribution. We start from a_{sym} values for Ca and Pb isotopes, as tabulated in Table III, coming from the DRHBc, AME2020, and FRDM2012 approaches. The numbers in the parentheses are rms deviations.

|	HFB	FRDM	Ref. [8]
a_s/a_v	1.11	1.41	1.13
	DRHBc		
Ca_a_{sym}^v_I	26.27 (2.28)	29.56 (2.83)	26.49 (2.31)
Ca_a_{sym}^v_II	26.25 (2.26)	29.53 (2.82)	26.47 (2.30)
Ca_a_{sym}^v_cor	27.17 (2.40)	30.57 (2.30)	27.40 (2.44)
Pb_a_{sym}^v_I	24.53 (0.71)	26.14 (0.80)	24.64 (0.71)
Pb_a_{sym}^v_II	26.57 (1.52)	28.31 (1.70)	26.69 (1.53)
Pb_a_{sym}^v_cor	27.80 (3.56)	29.63 (3.87)	27.93 (3.58)
	AME2020		
Ca_a_{sym}^v_I	27.49 (1.07)	31.36 (1.23)	27.74 (1.08)
Ca_a_{sym}^v_II	27.44 (1.06)	31.30 (1.23)	27.70 (1.07)
Pb_a_{sym}^v_I	24.24 (0.48)	25.93 (0.50)	24.36 (0.48)
Pb_a_{sym}^v_II	27.40 (0.90)	29.31 (0.99)	27.54 (0.91)
	FRDM2012		
Ca_a_{sym}^v_I	27.59 (1.08)	31.03 (1.47)	27.82 (1.10)
Ca_a_{sym}^v_II	27.57 (1.06)	31.00 (1.46)	27.79 (1.09)
Pb_a_{sym}^v_I	25.30 (0.72)	26.95 (0.61)	25.41 (0.72)
Pb_a_{sym}^v_II	27.34 (0.61)	29.13 (0.71)	27.46 (0.61)
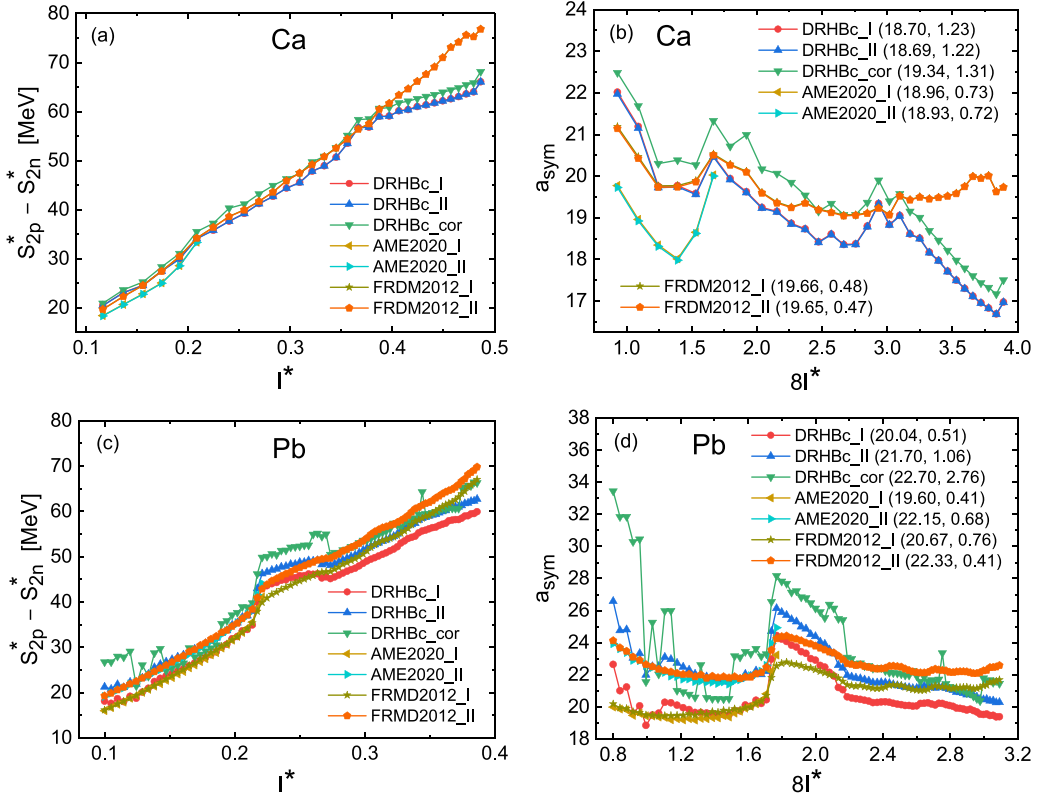
FIG. 6. $S_{2p}^* - S_{2n}^*$ (a) and a_sym (b) for Ca from DRHBc, AME2020, and FRDM2012, which correspond to the results in Figs. 5(c) and 5(d). $S_{2p}^* - S_{2n}^*$ (c) and a_sym (d) for Pb from DRHBc, AME2020, and FRDM2012, which correspond to the results in Figs. 4(c) and 4(d). The numbers in the parentheses of panels (b) and (d) are the central values and the rms deviations.

the a_s/a_v value. All of the results for a_sym^v are summarized in Table IV. For example, the values from FRDM2012 are larger than the values from other models. Final results of a_sym and a_sym^v with the ratio a_s/a_v extracted from the mass tables are tabulated and compared to other results [47,50] in Table V.

Here we mention that the uncertainty on the a_sym coming from the treatment of the Coulomb exchange term, which is estimated from the difference of the results by Set I and Set II,

is about 0.5 (0.1) MeV for Ca isotopes and 2.7 (1.6) MeV for Pb isotopes by DRHBc (FRDM).

E. Model independent approach

Since the ratio a_s/a_v in Eq. (5) is not well determined by other experimental observables, we take it as a free parameter and try to fix a_sym^v from the present a_sym in Pb and Ca isotopes. The final results are presented in Fig. 7.

TABLE V. Summary of a_sym, a_sym^v, and a_s/a_v for Ca and Pb with DRHBc, AME2020, and FRDM2012. Kim I and Kim II [50] are the results by using full range mass data, respectively, from DRHBc and AME2020. The Tian [47] results used AME2012 data [48].

	a_sym	a_sym^v	a_s/a_v
Ca (DRHBc)	18.7–[a] 19.3	26.2–27.4 (−30.6)[b]	1.10–1.13 (−1.41)[b]
Ca (AME2020)	18.9–19.0	27.4–27.7 (−31.4)	1.10–1.13 (−1.41)
Ca (FRDM2012)	19.6–19.7	27.5–27.8 (−31.3)	1.10–1.13 (−1.41)
Pb (DRHBc)	20.0–22.7	24.5–27.9 (−29.6)	1.10–1.13 (−1.41)
Pb (AME2020)	19.6–22.1	24.2–27.5 (−29.3)	1.10–1.13 (−1.41)
Pb (FRDM2012)	20.7–22.3	25.3–27.4 (−29.1)	1.10–1.13 (−1.41)
Kim I ($A = 208$)[c] [50]	21.36	27.85	1.38[d]
Kim II ($A = 208$) [50]	22.32	28.54	1.29[d]
Tian [47]	22.25	28.32	1.27[d]

[a]The range "–" comes from the Coulomb correction recipes in Table IV.

[b]The number in the parentheses is the result by the FRDM model, which shows a large $a_s/a_v = 1.41$.

[c]Kim I, Kim II, and Tian employed a formula $a_\mathrm{sym}(A) = a_\mathrm{sym}(1 - \kappa A^{1/3})$ with $\kappa = a_\mathrm{sym}^s/a_\mathrm{sym}^v$.

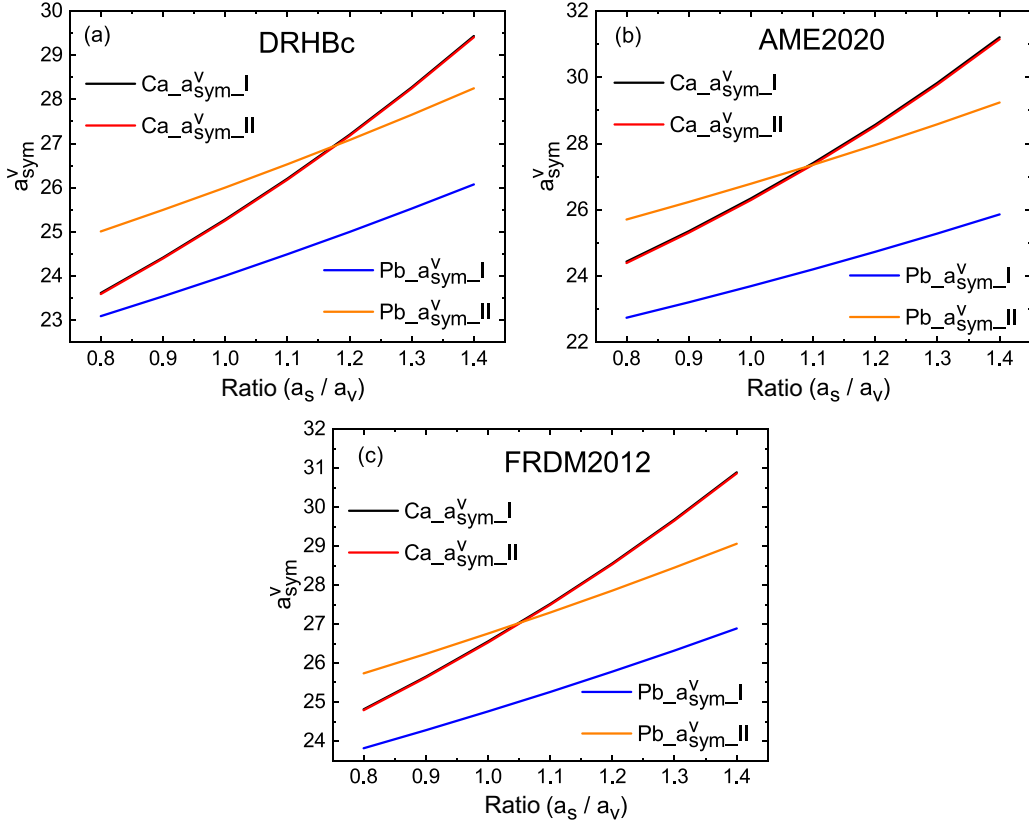[d]This value is $\kappa = a_\mathrm{sym}^s/a_\mathrm{sym}^v$.

FIG. 7. a_{sym}^{v} as a function of the ratio a_s/a_v for each nuclear mass model.

Since the Coulomb corrections were performed mainly for light and medium nuclei due to the paucity of mirror nuclei in heavy mass region, we consider only the results for Ca isotopes using Sets I and II, and those for Pb isotopes using only Set II (see the large rms deviation in the results using Set I in Table II). We note that the results from Ca isotopes using Sets I and II as well as those from Pb isotopes using Set II clearly show a crossing point at $a_{\mathrm{sym}}^{v} = 27$ MeV with $a_s/a_v = 1.1 \pm 0.1$. This result is almost model independent. The results from Pb isotopes using Set I deviate somehow; we should stress, however, that Set I is characterized by a larger rms deviation (cf. Table II). In addition, the Coulomb corrections may be more meaningful for light and medium mass nuclei, due to the paucity of mirror nuclei in the heavy mass region. These issues deserve further investigation.

IV. SUMMARY AND CONCLUSION

Our motivation, in the current study, was to highlight a new, alternative way of deducing the volume and surface symmetry energy coefficients of the nuclear mass formula. Despite many attempts to extract the symmetry energy from nuclear structure or reaction measurements, or from neutron star observation, the density dependence of the symmetry energy is still plagued by significant uncertainties. Symmetry coefficients of the mass formula can provide useful, complementary information. We have extracted them from the proton and neutron separation energies of Pb and Ca isotopes.

First, we deduced the symmetry energy coefficient, a_{sym}. We used the mass table provided by the DRHBc model. Our approach was applied starting from other mass tables. We used, then, the ratio a_s/a_v as an input to disentangle the volume and surface symmetry coefficients. Our final results for a_{sym} and a_{sym}^{v} values for Ca and Pb isotopes are tabulated in Table V. The a_{sym} values in the present work, obtained from the two-nucleon separation energies, are consistent with other results [47,50]. If we take the central value of a_{sym}^{v} results in Table V, when $a_s/a_v = 1.10$–1.13, we obtain a_{sym}^{v} as $a_{\mathrm{sym}}^{v} = 27.0_{-2.8}^{+0.96}$ considering the Pb isotopes, and $a_{\mathrm{sym}}^{v} = 27.0_{-0.8}^{+0.8}$ considering the Ca isotopes. The uncertainties stem from the treatment of the Coulomb interaction. The central value of a_{sym}^{v} turns out to be independent of the nuclear species; the larger $a_s/a_v = 1.41$ from FRDM is discarded here.

Since the ratio a_s/a_v is determined neither by nuclear theory nor by experimental data, we investigated a_{sym}^{v} by using the ratio a_s/a_v as a free parameter. Finally, we obtained $a_{\mathrm{sym}}^{v} = 27.0$ MeV, almost irrespective of nuclear model and isotopic chain. The ratio a_s/a_v is constrained also to be $a_s/a_v = 1.10$–1.13. From the deduction of the symmetry energy coefficients, a_{sym} and a_{sym}^{v}, we may discuss the symmetry energy as well as its slope parameter. We leave it as a future work.

Finally, we mention that the inclusion of Coulomb exchange energy or the lack thereof play a relevant role in the extraction of the symmetry energy. The exchange term is a physical effect that should be in principle considered using

some realistic approximation. A microscopic model with exact exchange term that can be applied to the whole isotope chart, including deformed and/or drip-line systems, is not available at present. DRHBc does not include a Fock term (i.e., is a Hartree model) formally; however, some part of exchange effects are implicitly taken into account when the parameters are optimized to reproduce the empirical binding energies. It is not easy to quantify this implicit effect. FRDM has different recipes to include the exchange effects that are discussed in our paper. As said elsewhere, in the present work we can only discuss the consequences either of the fact that models are different or of the fact that, specifically, they are different in the treatment of Coulomb exchange. Further investigation of the Coulomb exchange can be envisioned for future works.

[1] D. Adhikari *et al.*, Phys. Rev. Lett. **126**, 172502 (2021).

[2] J. Zenihiro *et al.*, Phys. Rev. C **82**, 044611 (2010).

[3] V. E. Starodubsky and N. M. Hintz, Phys. Rev. C **49**, 2118 (1994).

[4] L. Ray, W. R. Coker, and G. W. Hoffmann, Phys. Rev. C **18**, 2641 (1978); L. Ray, *ibid.* **19**, 1855 (1979); G. W. Hoffmann *et al.*, *ibid.* **21**, 1488 (1980).

[5] J. Zenihiro *et al.*, arXiv:1810.11796.

[6] X. Roca-Maza and N. Paar, Prog. Part. Nucl. Phys. **101**, 96 (2018).

[7] C. F. v. Weizsöcker, Z. Phys. **96**, 431 (1935).

[8] D. Lunney, J. M. Pearson, and C. Thibault, Rev. Mod. Phys. **75**, 1021 (2003).

[9] K. Zang, M.-K. Cheoun, Y.-B. Choi, P. S. Chong, J. Dong, Z. Dong *et al.*, At. Data Nucl. Data Tables **144**, 101488 (2022).

[10] P. Möller, A. J. Sierk, T. Ichikawa, and H. Sagawa, At. Data Nucl. Data Tables **109-110**, 1 (2016).

[11] M. Wang, W. J. Huang, F. G. Kondev, G. Audi, and S. Naimi, Chin. Phys. C **45**, 030003 (2021).

[12] https://www-nds.iaea.org/amdc/.

[13] https://t2.lanl.gov/nis/molleretal/publications/ADNDT-FRDM2012.html.

[14] J. D. Walecka, Ann. Phys. (NY) **83**, 491 (1974).

[15] J. Boguta and R. Bodmer, Nucl. Phys. A **292**, 413 (1977).

[16] S.-G. Zhou, J. Meng, P. Ring, and E.-G. Zhao, Phys. Rev. C **82**, 011301(R) (2010).

[17] L. Li, J. Meng, P. Ring, E.-G. Zhao, and S.-G. Zhou, Phys. Rev. C **85**, 024312 (2012).

[18] K. Zhang *et al.*(DHRBc Mass Table Collaboaration), Phys. Rev. C **102**, 024314 (2020).

[19] C. Pan, K. Y. Zhang, P. S. Chong, C. Heo, M. C. Ho, J. Lee *et al.*, Phys. Rev. C **104**, 024331 (2021).

[20] K. Zhang, X. He, J. Meng, C. Pan, C. Shen, C. Wang, and S. Zhang, Phys. Rev. C **104**, L021301 (2021).

[21] C. Pan, K. Zhang, and S. Zhang, Int. J. Mod. Phys. E **28**, 1950082 (2019).

[22] X.-X. Sun, J. Zhao, and S.-G. Zhou, Phys. Lett. B **785**, 530 (2018).

[23] X.-X. Sun, J. Zhao, and S.-G. Zhou, Nucl. Phys. A **1003**, 122011 (2020).

[24] E. J. In, P. Papakonstantinou, Y. Kim, and S.-W. Hong, Int. J. Mod. Phys. E **30**, 2150009 (2021).

[25] Z. H. Yang *et al.*, Phys. Rev. Lett. **126**, 082501 (2021).

[26] X.-X. Sun, Phys. Rev. C **103**, 054315 (2021).

[27] X.-X. Sun and S.-G. Zhou, Phys. Rev. C **104**, 064319 (2021).

[28] X.-X. Sun and S.-G. Zhou, Sci. Bull. **66**, 2072 (2021).

[29] J. Meng and P. Ring, Phys. Rev. Lett. **77**, 3963 (1996).

[30] J. Meng, Nucl. Phys. A **635**, 3 (1998).

[31] S.-G. Zhou, J. Meng, and P. Ring, Phys. Rev. C **68**, 034323 (2003).

[32] L. M. Robledo, R. Bernard, and G. F. Bertsch, Phys. Rev. C **86**, 064313 (2012).

[33] P. W. Zhao, Z. P. Li, J. M. Yao, and J. Meng, Phys. Rev. C **82**, 054319 (2010).

[34] J. Dobaczewski, W. Nazarewicz, T. R. Werner, J. F. Berger, C. R. Chinn, and J. Decharge, Phys. Rev. C **53**, 2809 (1996).

[35] Y. Tian, Z. Y. Ma, and P. Ring, Phys. Lett. B **676**, 44 (2009).

[36] S. Kim, M.-H. Mun, M.-K. Cheoun, and E. Ha, Phys. Rev. C **105**, 034340 (2022).

[37] J. Decharge and D. Gogny, Phys. Rev. C **21**, 1568 (1980).

[38] M. Serra, A. Rummel, and P. Ring, Phys. Rev. C **65**, 014304 (2001).

[39] T. Nikšić, N. Paar, D. Vrentano, and P. Ring, Comput. Phys. Commun. **185**, 1808 (2014).

[40] A. V. Afanasjev, S. E. Agbemava, D. Ray, and P. Ring, Phys. Lett. B **726**, 680 (2013).

[41] A. V. Afanasjev and O. Abdurazakov, Phys. Rev. C **88**, 014320 (2013).

[42] D. Vretenar, A. V. Afanasjev, G. A. Lalazissis, and P. Ring, Phys. Rep. **409**, 101 (2005).

[43] S. E. Agbemava, A. V. Afanasjev, D. Ray, and P. Ring, Phys. Rev. C **89**, 054320 (2014).

[44] X. W. Xia *et al.*, At. Data Nucl. Data Tables **121-122**, 1 (2018).

[45] A. Trzcinska, J. Jastrzebski, P. Lubinski, F. J. Hartmann, R. Schmidt, T. von Egidy, and B. Klos, Phys. Rev. Lett. **87**, 082501 (2001).

[46] N. Wang, L. Ou, and M. Liu, Phys. Rev. C **87**, 034327 (2013).

[47] J. Tian, H. Cui, K. Zheng, and N. Wang, Phys. Rev. C **90**, 024313 (2014).

[48] G. Audi G. M. Wang, A. H. Wapstra, F. G. Kondev, M. MacCormick, X. Xu, and B. Pfeiffer, Chin. Phys. C **36**, 1287 (2012).

[49] V. M. Strutinsky, Nucl. Phys. A **95**, 420 (1967).

[50] S. Kim, D. Jang, S. Choi, T. Miyatsu, and M.-K. Cheoun, arXiv:2307.0518.